Shielding Design for High-Frequency Wireless Power Transfer System for EV Charging with Self-Resonant Coils

Ruiyang Qin
Min H. Kao Department of Electrical Engineering and Computer Science
The University of Tennessee, Knoxville
Knoxville, TN, USA
rqin1@vols.utk.edu

Jie Li
Min H. Kao Department of Electrical Engineering and Computer Science
The University of Tennessee, Knoxville
Knoxville, TN, USA
jli94@vols.utk.edu

Jingjing Sun
Min H. Kao Department of Electrical Engineering and Computer Science
The University of Tennessee, Knoxville
Knoxville, TN, USA
jsun30@vols.utk.edu

Daniel Costinett
Min H. Kao Department of Electrical Engineering and Computer Science
The University of Tennessee, Knoxville
Knoxville, TN, USA
daniel.costinett@utk.edu

2022 IEEE Energy Conversion Congress and Exposition (ECCE) | 978-1-7281-9387-8/22/$31.00 ©2022 IEEE | DOI: 10.1109/ECCE50734.2022.9948194

***Abstract*—This paper provides a complete design solution for a 6.6 kW wireless power transfer system based on compact self-resonant (SR) coils with shielding considered. The high frequency parasitic capacitance introduced by the shielding material is analyzed in detail, and a shielding geometry optimization method is proposed. Using ferrite for shielding and a PTFE spacer, the total thicknesses of coils are only 11.4 mm and 7.4 mm for the transmitter and receiver, respectively. The system is validated with fabricated SR coils, achieving 92.3% DC-DC efficiency and 7.1 kW/dm^3 volumetric power density. This paper demonstrates the first 6.6-kW WPT system for EV charging using compact self-resonant coils at MHz with practical shielding implementation.**

Keywords—shielding design, self-resonant coil, multi-layer spiral coil, wireless power transfer, electric vehicle charging

I. Introduction

With the increasing interest in lightweight and compact wireless charging systems for electric vehicles, high-frequency wireless power transfer (WPT) systems have drawn more attention nowadays. Multiple coil design approaches at MHz have been reported, using various type types of self-resonant (SR) coils [1]-[6]. Without the need for external lumped capacitors for compensation, higher power density can be achieved using SR coils, with greatly relieved thermal stress on capacitors due to the distributed capacitance [7][8].

However, when installed in an EV, any charging coils will exert high leakage magnetic field, causing excessive eddy current loss on the structural elements of the vehicle chassis like carbon steel or aluminum alloys. To avoid such high power loss on the chassis and also to attenuate stray field in surrounding areas, proper shielding is required for any coil, including SR coils. To reduce the leakage magnetic field, different shielding approaches have been studied, mainly including conductive shielding [9][10], magnetic shielding [11], and active shielding [12]-[14]. The conductive shielding utilizes the induced opposing magnetic field in the metal plate to counteract the coil fringing field. The conductive shield may also be used as heatsink and provide structural strength for the whole coil assembly. Different metal materials including copper and aluminum are compared in [9] to study the effectiveness of shielding. Instead of counteracting, magnetic shielding using ferrite concentrates the flux around the coil, which reduces the leakage flux while increasing the coil coupling coefficient. A wing shape ferrite is used in [11] for better shielding performance.

Conductive shielding and magnetic shielding are often applied together. SAE J2954 contains standards for the typical size and dimension of shielding using metal plate and ferrite [15]. With additional reactive *LC* resonant coils around the main coil, the fringing field can also be actively cancelled [12][13]. In [14], the phases of windings currents are controlled to minimize stray field. Still, additional components and a more complicated control algorithm are required for active shielding and may increase the cost and size of the system.

Prior work focuses on the study of shielding design for the WPT systems with Litz windings in a relatively low frequency range below 100 kHz. No work reported so far discusses the shielding consideration for high frequency WPT systems with SR coils for EV applications. Of all the self-resonant coils in [1]-[8], only the structures from [3][8] reach high power delivery at kW level for potential EV application as demonstrated in [16]-[18]. The study in [19] explores the possibility of shielding MHz-range SR coil using a resonant reactive coil, but the shielding effect is limited.

In this paper, a complete shielding design solution is provided based on the previously-proposed 3 MHz multi-layer non-uniform SR coils, shown in Fig. 1 [17]. With the existence of both ferrite and aluminum, the impact of shielding on the multi-layer SR coil at MHz range is analyzed in detail. Design guidelines are provided for the ferrite geometries, and an integrated design optimization process is proposed within the WPT system. To verify the design result, a shielding structure is assembled based on the previously reported multi-layer non-uniform SR coils and tested up to 6.6 kW. This paper validates the performance of high frequency WPT system with SR coils considering the practical shielding requirement for wireless

978-1-7281-9387-8/22/$31.00 ©2022 IEEE

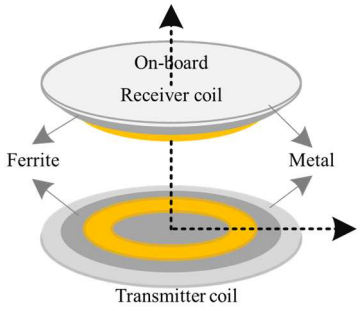

Fig. 1. Proposed shielding structure for WPT system with SR coils

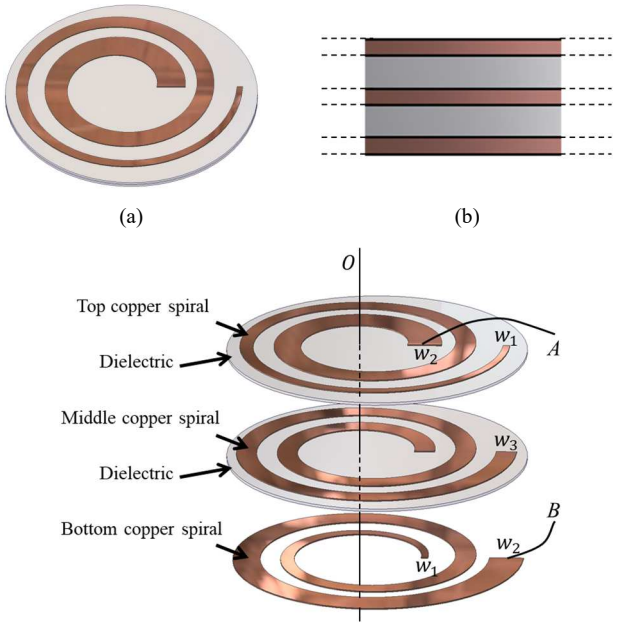

Fig. 2. Three-layer non-uniform SR coil structure (a) 3D view (b) side view (c) exploded 3D view [18]

charging deployment on EVs.

The paper is organized as follows. Section II investigates the ferrite and metal impacts on the multi-layer SR coil with fast 2D magnetic field simulator. Section III presents the design guidelines for shielding geometry, with a focus on the impact of parasitic capacitance with ferrites at MHz range. Section IV gives the systematic shielding geometry optimization process. Section V presents the complete fabrication process and test results of the high frequency WPT system with shielded SR coils. Section VI concludes the paper.

II. Shielding Requirement for Self-Resonant Coils Deployment on EVs

The structure of the proposed multi-layer non-uniform SR coil with series resonance is shown in Fig. 2. Three layers of copper spiral traces are stacked vertically, with two equal-thickness layers of dielectric material sandwiched between. The current flows from terminal A on the top layer to the terminal B on the bottom layer, gradually transition through both dielectric layers in series. The total current is distributed over three layers of copper, controlled by the non-uniform copper width w_1, w_2, and w_3. Together with the inductance from the spiral coils, the three-layer coil works as a series L-C resonant network. The proposed SR coil has the advantages of high inductance and high quality factor, providing a lightweight and low-cost solution for high power, high frequency wireless EV charging [18].

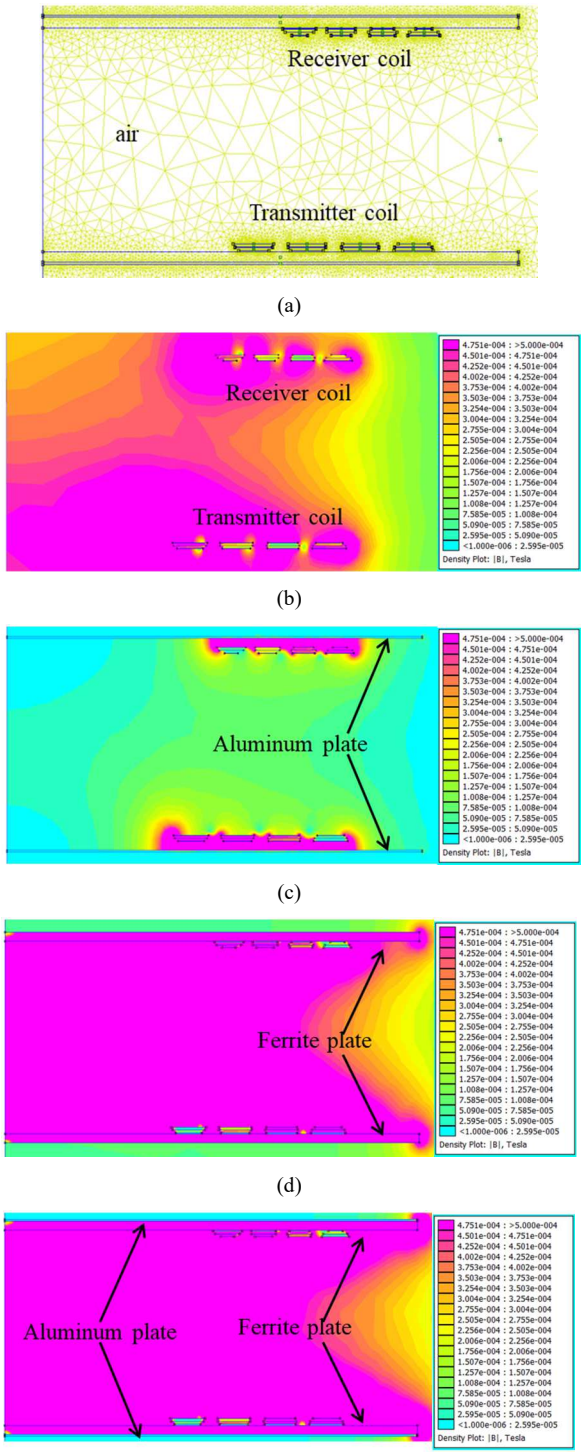

Fig. 3. FEMM based 2D magnetic field simulation for a 6.6 kW system with proposed multi-layer SR coils (a) meshing setup in FEMM (b) magnetic field without shielding (c) magnetic field with aluminum shielding (d) magnetic field with ferrite shielding (e) magnetic field with ferrite + aluminum shielding

A fast 2D magnetic simulation is conducted first using FEMM [20] to illustrate the shielding challenge when the SR coils are deployed for EV charging. With the 2D axi-

TABLE I
COIL INDUCTANCE AND COUPLING COMPARISON

Shielding method	Inductance [μH]		Quality factor @3MHz		Mutual inductance [μH]	Coupling coefficient
	TX	RX	TX	RX		
No shielding	5.24	6.82	426	434	1.66	0.278
Al. shielding	0.83	1.14	90	94	0.02	0.021
Fe. shielding	10.5	13.5	539	595	4.98	0.418
Fe. + Al.	10.0	12.8	534	573	4.39	0.388

Shielding method	Coil-coil max. efficiency	Leakage field 10 mm above RX [μH]	Al. weight [kg]	Fe. weight [kg]
No shielding	98.34%	300	0	0
Al. shielding	37.01%	0.02	0.9	0
Fe. shielding	99.16%	73	0	7.7
Fe. + Al.	99.07%	0.41	0.9	7.7

symmetrical meshing setup shown in Fig. 3(a), Fig. 3(b)-(d) gives the magnetic field distribution for the 6.6 kW system with the proposed multi-layer SR coils. The coil radius is 200 mm with 17.9 A transmitter coil current, 11.9 A receiver coil current, 3.125 MHz frequency, and 100 mm airgap between two coils as demonstrated in SR coil design from [18]. Clearly, high fringing field exists at top and bottom of coils as shown in Fig. 3(b), which will induce eddy current loss at surrounding metal objects on the vehicle and destroy the coupling of coils.

One straightforward approach to shielding is to apply conductive metal, as shown in Fig. 3(c). Identical 1 mm thick, 225 mm radius aluminum plates are placed 5 mm away from the coils. The magnetic field outside the plates is well constrained at several μT level. However, the opposing magnetic field generated by the eddy current that is induced on the metal plate alters the field distribution around the coils, and the coil inductance and coupling are greatly reduced, leading to a significant drop in coil-to-coil maximum efficiency as summarized in TABLE I.

In Fig. 3(d) ferrites are instead used to channel the flux around the coil. Most of the flux outside the two coils is now contained within the ferrite cores, with a boost in both inductance and coupling coefficient. Still, the leakage magnetic field above the receiver coil is much larger compared to the aluminum shielding case, with much higher weight required for shielding.

Based on the case study above, ferrite cores and aluminum plates are needed together for shielding in a complete high frequency SR coil pad design as shown in Fig. 3(e), with ferrites to channel the flux around the coil, increasing the inductance and coupling coefficient, and aluminum plates to shield the remaining stray field and also provide the mechanical structure to mount the coil on the vehicle. To have efficient utilization of shielding material, proper design optimization is needed to quantify the trade-off between shielding weight and performance. In the next section, a more detailed analysis is provided, giving shielding design guidelines for optimal power density.

III. SHIELDING DESIGN GUIDELINES CONSIDERING THE PARASITIC CAPACITANCE WITH FERRITES

Compared to the conventional 85 kHz system, shielding design for high frequency SR coils faces more challenges, including the coil performance degradation caused by the parasitic parallel capacitance between winding turns, which needs to be addressed before deploying the SR coils on EVs. There are multiple studies for WPT shielding design using ferrites and metal plates, yet no work has been proposed to study the shielding impact on multi-turn SR coils suitable for EV application in the current literature.

Any SR coil or traditional lumped-capacitance coil exhibits a parasitic parallel capacitance due to the turn-to-turn and turn-to-shield capacitances. In low-frequency, sub-MHz, designs the resonance introduced by this parallel capacitance is often orders of magnitude higher-frequency than the series resonant frequency, and minimally impacts operation. For the proposed high frequency SR coils, the parallel resonance introduced by the shielding material can be close to the series resonant frequency and therefore needs to be considered during the design process for its impact on the coil performance.

The electric potential is simulated between two adjacent turns of the coil as shown in Fig. 4. Below the coil, a 2 mm thick layer of DMR51W ferrite material [21] and 1 mm thick sheet of Al are used for shielding. To tune the parasitic capacitance, PTFE is selected as a filler material between the coil and ferrites, which is low-cost and available for a wide range of thicknesses. It has 2.1 dielectric constant and 0.0003 dielectric loss tangent.

Between the two adjacent copper traces, there are four parasitic capacitances which are connected in series: C_1 and C_2 formed between the aluminum plate and copper trace on the left, C_3 and C_4 formed between the aluminum plate and copper trace on the right. The total equivalent capacitance is

$$C_{eq} = \frac{1}{\frac{1}{C_1}+\frac{1}{C_2}+\frac{1}{C_3}+\frac{1}{C_4}} \quad (1)$$

Each capacitance is calculated using potential-theoretic method based on Fourier series expansion for the electric field [22],

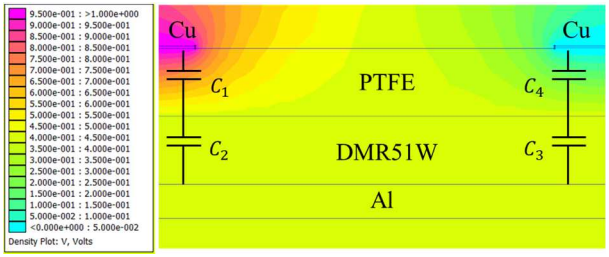

Fig. 4. FEMM based 2D electric field simulation for the coil with shielding

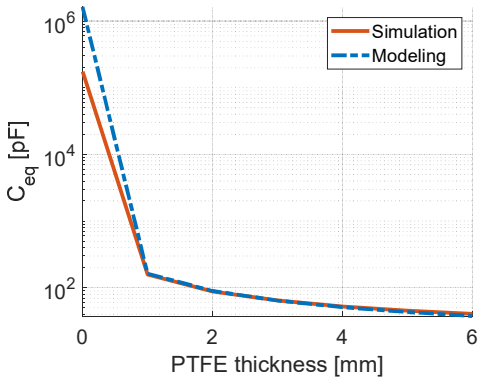

Fig. 5. Equivalent capacitance between two adjacent coil turns

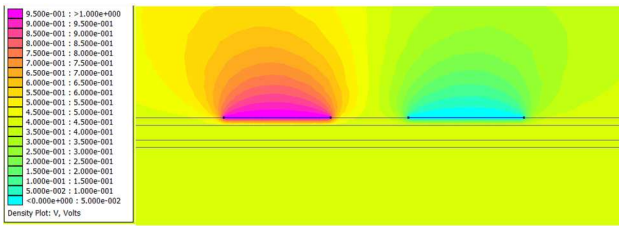

(a)

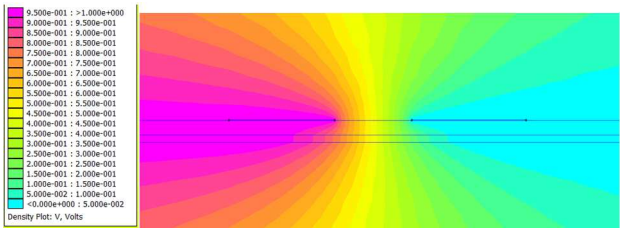

(b)

Fig. 6. Electric potential plot comparison (a) PTFE thickness = 1mm (b) no PTFE layer

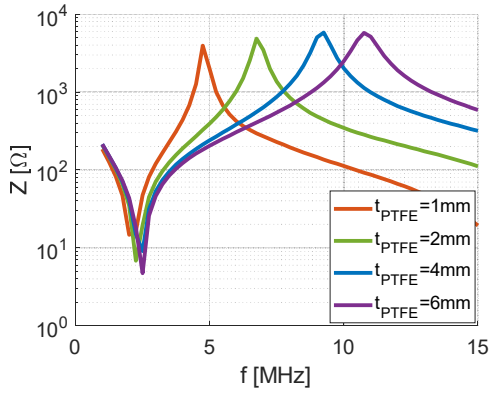

Fig. 7. Coil impedance plot with varying PTFE thickness in HFSS

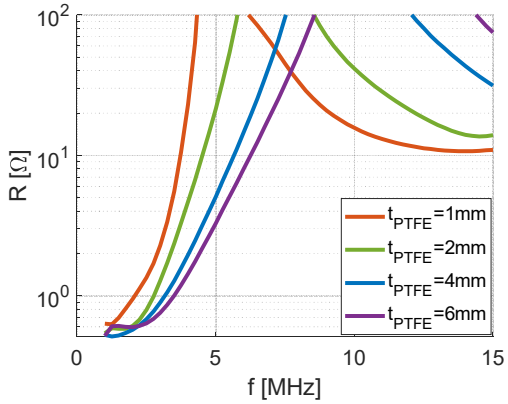

Fig. 8. Coil ESR plot with varying PTFE thickness in HFSS

$$\phi(x,y) = \sum_{n=1}^{\infty} A_n \sin(k_n y) e^{-k_n x} \quad (2)$$

where A_n and k_n are constants determined by the boundary conditions for electric potential around the parallel plate.

Note that C_1 and C_4 are much smaller than C_2 and C_3 if the thickness of PTFE and DMR51W are comparable. This is caused by the very high dielectric constant for DMR51W, close to 40000, at MHz range (dielectric constant = 38700 @ 3 MHz) [23]. In other words, the total equivalent capacitance is dominated by the capacitance contributed by the PTFE layer.

With the varying thickness of the PTFE as shown in Fig. 5, the equivalent capacitance between two coil turns can be tuned accordingly. If the PTFE layer is too thick, although the value of the equivalent capacitance drops to several pF and the impact of the parallel resonance can be ignored, the power density of the coil is largely sacrificed considering the increased weight and size of PTFE layer.

On the other hand, if the PTFE layer is designed to be too thin, the power density of the coil pad is improved, but there will be high equivalent parallel capacitance, leading to a lower parallel resonant frequency and negative impact on the coil performance. Note that when the thickness of PTFE layer is zero (no PTFE layer exists), the pattern of electric potential changes completely as shown in Fig. 6(b) due to the conductivity of the ferrites. Accordingly, a minimal electrical insulation is always required between the copper traces and ferrites in the final assembly.

To provide quantitative results of the change of resonant frequency and ESR, a 3D electromagnetic simulation is performed. Fig. 7 and Fig. 8 give the HFSS simulation results of the coil impedance and ESR, respectively, with varying PTFE thickness. The original coil without shielding has 5 μH inductance and 3 MHz resonant frequency.

With the increasing PTFE thickness, the parasitic capacitance caused by the shielding continues to decrease, leading to a higher parallel resonant frequency and lower coil ESR, which verifies the analysis of the lumped element model. The simulation results with different PTFE thickness are summarized in TABLE II. With larger parasitic capacitance, both coil quality factor and series resonant frequency are decreased.

In order to quantitatively evaluate the shielding impact on the coil quality factor, and to facilitate the best trade-off between the electrical performance and the power density, the shielding structure is optimized together with the system design based on the 3D FEA simulation results, as explained in the next section.

IV. Systematic Shielding Geometry Optimization

Since the shielding design will strongly impact the trade-off between system efficiency and power density, a system-level design optimization procedure is proposed to locate the optimal design of the shielding geometry. The inverter and rectifier are modeled and designed in [18], with GaN Systems GS66516T 650 V GaN transistors and CREE C4D08120E 1200 V SiC Schottky diodes implementing the high frequency inverter and rectifier, respectively. The system circuit diagram is shown in Fig. 9.

The zero-voltage-switching (ZVS) is guaranteed by tuning the switching frequency f_s around the coil resonant frequency f_0

TABLE II
Resonant Frequency and ESR of Coil with Varying PTFE Thickness

PTFE thickness [mm]	1	2	3	4
Series resonant frequency [MHz]	2.12	2.31	2.40	2.45
Parallel resonant frequency [MHz]	4.89	6.85	9.18	10.82
ESR [Ω]	1.030	0.704	0.657	0.632

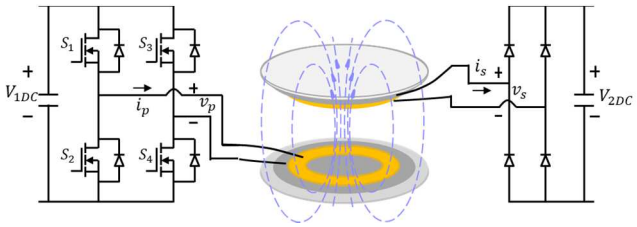

Fig. 9. WPT system circuit diagram with proposed SR coils

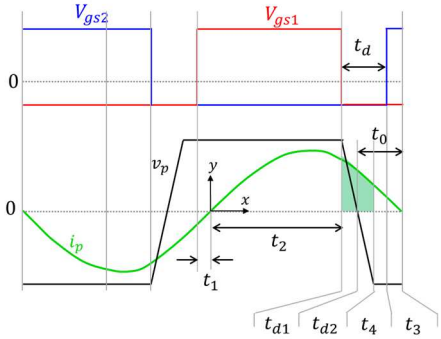

Fig. 10. Waveforms for inverter gate signals V_{gs1}, V_{gs2}, and inverter switching node voltage v_p, current i_p within one switching cycle

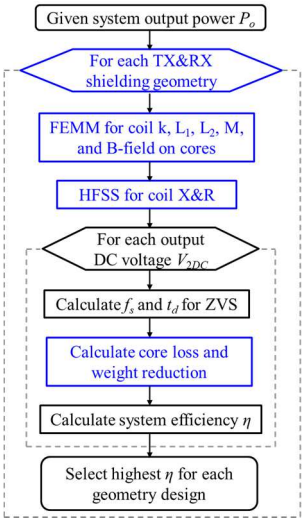

Fig. 11. Design flow chart for shielding optimization

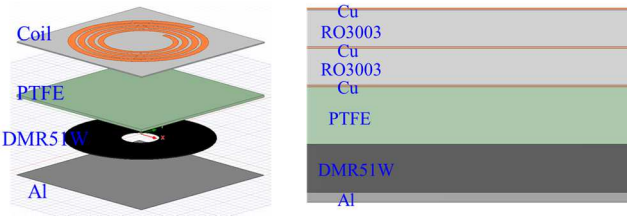

(a) (b)

Fig. 12. Shielding structure for optimization (a) 3D overview (b) side view with detailed material information

with the shielding impact considered. As shown in Fig. 10, a slightly positive phase shift is needed between the switching node voltage v_p and current i_p to allow enough charge, $2Q_{oss}$, to complete ZVS process of one phase leg.

For the completion of ZVS, time intervals t_{d1} and t_{d2} need to fulfill

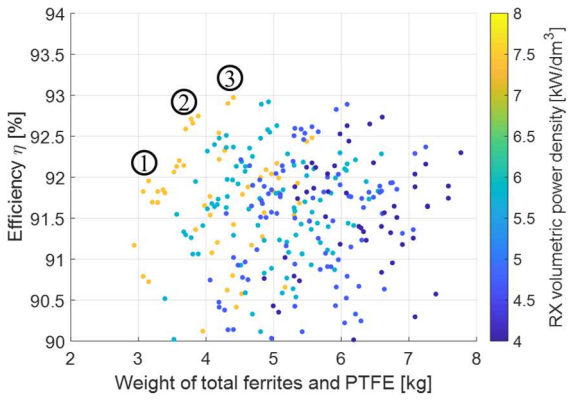

Fig. 13. System optimization result

TABLE III
DESIGN PARAMETERS ON CASES ON THE PARETO FRONT

No.	η [%]	Fe [kg]	PTFE [kg]	Fe thickness [mm]		PTFE thickness [mm]		Fe inner radius [mm]	
				TX	RX	TX	RX	TX	RX
1	91.95	2.18	0.97	2	2	2	2	75	25
2	92.71	2.27	1.51	2	2	4	2	50	25
3	92.97	2.33	2.08	2	2	6	2	25	25

$$Q_{oss} = \int_{\frac{T_s}{2}-t_0-t_{d1}}^{\frac{T_s}{2}-t_0} \sqrt{2} I_p \sin(\omega_s t) dt \quad (3)$$

$$Q_{oss} = \int_{\frac{T_s}{2}-t_0}^{\frac{T_s}{2}-t_0+t_{d2}} \sqrt{2} I_p \sin(\omega_s t) dt \quad (4)$$

where I_p is the RMS value of i_p, and the switching dead time t_d is selected such that

$$t_{d1} + t_{d2} \le t_d \le t_{d1} + t_0 \quad (5)$$

The system design flow chart for shielding optimization is summarized in Fig. 11. To relieve the calculation burden from 3D electromagnetic simulation, faster 2D FEMM-based simulation is first used to calculate the inductance and coupling coefficient of the coils under the influence of the shielding, while 3D HFSS-based electromagnetic simulation is used to calculate the coil ESR considering the impact from the parallel parasitic capacitance and the dielectric loss from ferrites, which cannot be found by 2D FEMM magnetostatic simulation. The core loss of the ferrites is estimated by the magnetic field distribution captured from FEMM simulation and core loss data from the datasheet provided by the vendor [21]. Together with the WPT system model proposed in [18], the highest system efficiency is calculated for each shielding geometry.

Parameters including Ferrite thickness [2 mm, 4 mm], ferrite disc inner radius [25 mm, 50 mm, 75 mm], and PTFE thickness [2 mm, 4 mm, 6 mm] are swept, and corresponding HFSS simulation results are incorporated into the WPT system model to calculate the system efficiency, weight of shielding materials, and shielded coil volumetric power density. The dimension of the Al plate is 18" x 18" with 0.016" thickness. The outer radius of the ferrite plate is selected to be the same as the coil pad, 200 mm, to channel the flux from all coil traces. The shielding structure is shown in Fig. 12.

Totally 324 cases of shielding design are simulated and

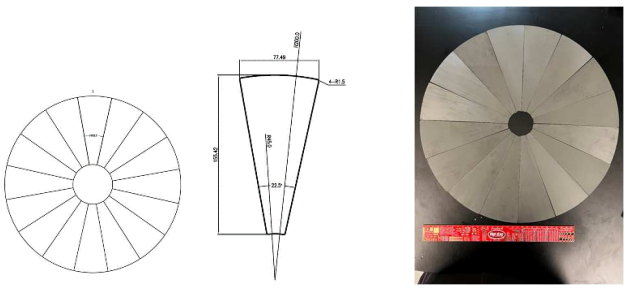

(a) (b)

Fig. 14. DMR51W cores (a) drawing of fabrication plan (b) fabricated ferrite cores

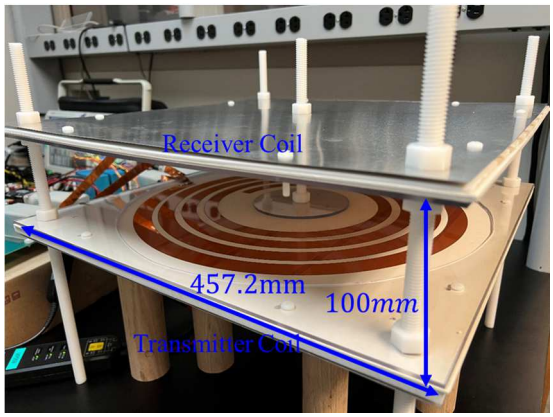

Fig. 15. Complete assembly for coils with shielding

optimized, and the sweeping result for system efficiency is shown in Fig. 13. The *x*-axis shows the total weight of ferrites and PTFE for two coils, and the color of the dot represents the volumetric power density based on the RX coil volume, including copper, RO3003 laminates, ferrites, and PTFE spacer. The detailed specifications of three cases on the Pareto front are summarized in TABLE III. Case No. 3 is selected for the prototype build considering the balance between efficiency, power density and the cost of magnetic material. For the ferrite, 2 mm thickness DMR51W with 25 mm inner radius and 200 mm outer radius is applied for both the transmitter side and receiver side. For the airgap filling material, 6 mm and 2 mm thickness PTFE are applied on the transmitter side and receiver side, respectively.

TABLE IV
SHIELDED COIL PADS BILL OF MATERIALS

Name	Part number	Quantity	Dimension [mm]	Total weight [kg]
		TX coil pad		
Coil ceramics	RO3003	2	457.2x457.2x1.5	1.317
Copper	RO3003	NA	4 turns, 2oz	0.116
Ferrite	DMR51W	16	155.42x77.49	1.163
PTFE	McMaster 8545K46	1	457.2x457.2x6.35	2.247
Aluminum	McMaster 6061	1	457.2x457.2x0.4064	0.229
Polycarbonate	McMaster 8574K53	1	457.2x457.2x3.175	0.309
Total				5.381
		RX coil pad		
Coil ceramics	RO3003	2	457.2x457.2x1.5	1.317
Copper	RO3003	NA	3-layer, 4 turns, 2oz	0.088
Ferrite	DMR51W	16	155.42x77.49	1.163
PTFE	McMaster 8545K46	1	457.2x457.2x2.381	0.856
Aluminum	McMaster 6061	1	457.2x457.2x0.4064	0.229
Polycarbonate	McMaster 8574K53	1	457.2x457.2x3.175	0.450
Total				4.103

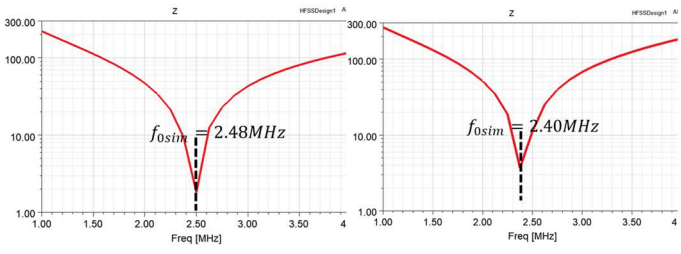

(a) (b)

Fig. 16. Impedance results of shielded coil in HFSS simulation (a) transmitter coil (b) receiver coil

V. SHIELDING HARDWARE ASSEMBLY AND EXPERIMENTAL VERIFICATION

To validate the above design methodology, a complete WPT system with shielded SR coils is fabricated and tested. Based on the manufacturing capabilities of the vendor, 16 pie-shaped ferrite cores are fabricated and assembled to make one complete ferrite plate of a coil as shown in Fig. 14. Each pie-shaped core has 22.5° center angle with approximately 155.42 mm in length.

Fig. 15 gives the final complete assembly for coils with shielding, with 100 mm airgap between two coil pads. Including the PTFE spacer, the thickness of the transmitter and receiver coil pads are only 11.4 mm and 7.4 mm, respectively. The complete bill of materials for the coil pad assembly is shown in TABLE IV, including the aluminum back plate and polycarbonate plate for clamping. The major weight contributor is the PTFE spacer, and only 1.2 kg ferrite plate is used for each coil. With smaller thickness of PTFE on the receiver side, the weight of receiver coil pad is 20% lighter than the transmitter side.

The impedances of the shielded coils are plotted in Fig. 16, and the corresponding characterization results are summarized in TABLE V. Due to the existence of the ferrites, the coil inductance has increased by about 30% compared with the original coil without shielding. In addition, compared with the tested result using an impedance analyzer, there is less than 5% error from the simulation results for parameters including series resonant frequency, inductance, capacitance, and coupling coefficient. Core loss is not included in the HFSS simulation and is calculated separately using the vendor's datasheet. Since core loss is nonlinear, measured coil ESR under small signal bias using an impedance analyzer is only used for fast characterization of the magnetic material, which gives relatively large error compared to the HFSS simulation result.

The hardware setup for the system is shown in Fig. 17, with 6.6 kW power test result shown in Fig. 18. At 2.439 MHz switching frequency, 40 ns deadtime, and 80 Ω load resistor, the system is tested up to 6.6 kW, with 92.3% dc-dc efficiency.

TABLE V
SHIELDED SR COILS CHARACTERIZATION AND COMPARISON

	HFSS simulation (core loss not included)	Impedance analyzer
	TX coil pad	
f_0 [MHz]	2.48	2.42
L [μH]	7.26	7.72
C [pF]	567.8	562.9
R [Ω]	0.593	0.639
	RX coil pad	
f_0 [MHz]	2.40	2.42
L [μH]	10.12	9.84
C [pF]	435.6	438.8
R [Ω]	0.957	0.878
	Two coil pads	
k	0.278 (FEMM)	0.272

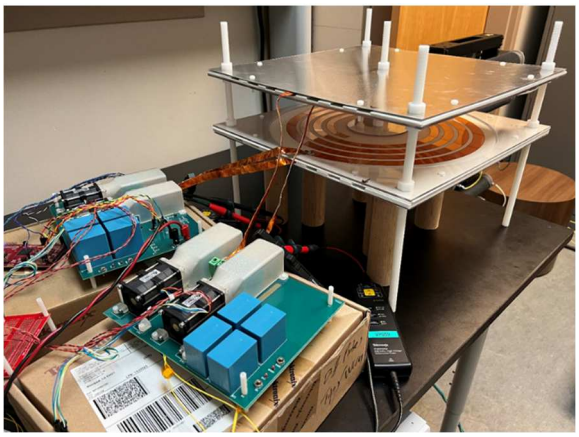

Fig. 17. WPT system with shielded SR coils

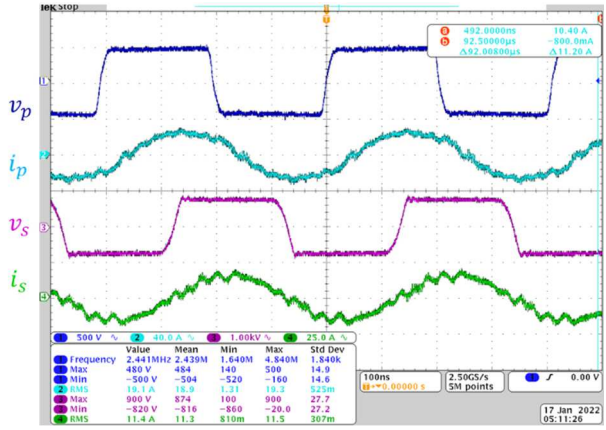

Fig. 18. 6.6 kW system power test waveforms

TABLE VI
SYSTEM TESTED RESULT COMPARISON

	Input voltage [V]	Transmitter current I_p [A]	Load voltage V_{2DC} [V]	Receiver current I_s [A]	Efficiency η
Model	494.7	17.8	726.6	11.5	93.1%
Test	471.8	19.1	733.6	11.4	92.3%

The detailed tested parameter comparison in TABLE VI confirms the validity of the optimization process in the previous section.

VI. CONCLUSIONS

This paper provides a complete design solution for 6.6 kW WPT system based on the proposed SR coils with shielding considered. The high frequency parasitic capacitance introduced by the shielding material is considered, and a shielding geometry optimization method is proposed. Using ferrite for shielding and a PTFE spacer, the total thickness of coils are only 11.4 mm and 7.4 mm for the transmitter and receiver, respectively. The system is validated with fabricated SR coils, achieving 92.3% DC-DC efficiency and 7.1 kW/dm^3 volumetric power density. This paper demonstrates the first 6.6 kW WPT system for EV charging using compact self-resonant coils at MHz with practical shielding implementation.

ACKNOWLEDGMENT

This research is supported by II-VI Foundation Block-Gift Graduate Research Program.

This work also made use of Engineering Research Center Shared Facilities supported by the Engineering Research Center Program of the National Science Foundation and the Department of Energy under NSF Award Number EEC-1041877 and the CURENT Industry Partnership Program.

REFERENCES

[1] de Miranda, C. M. and S. F. Pichorim, "A Self-Resonant Two-Coil Wireless Power Transfer System Using Open Bifilar Coils," *IEEE Transactions on Circuits and Systems II: Express Briefs* 64(6): 615-619, 2017.

[2] Chen, K. and Z. Zhao, "Analysis of the Double-Layer Printed Spiral Coil for Wireless Power Transfer," *IEEE Journal of Emerging and Selected Topics in Power Electronics* 1(2): 114-121, 2013.

[3] Stein, A. L. F., et al., "High-Q self-resonant structure for wireless power transfer," *IEEE Applied Power Electronics Conference and Exposition*, 3723-3729, 2017.

[4] Li, J. and D. Costinett, "Analysis and design of a series self-resonant coil for wireless power transfer," *IEEE Applied Power Electronics Conference and Exposition*, 1052-1059, 2018.

[5] P. H. McLaughlin, Y. Wu, C. R. Sullivan and J. T. Stauth, "Modeling and Design of Planar-Spiral Merged-LC Resonators in a Standard CMOS Process," *2020 IEEE 21st Workshop on Control and Modeling for Power Electronics (COMPEL)*, Aalborg, Denmark, 2020, pp. 1-8.

[6] Son, H. C., et al., "Self-Resonant Coil with Coaxial-like Capacitor for Wireless Power Transfer," *Asia-Pacific Microwave Conference* 2011: 90-93.

[7] Kyaw, P. A., et al., "High-Q resonator with integrated capacitance for resonant power conversion," *IEEE Applied Power Electronics Conference and Exposition*, 2519-2526, 2017.

[8] R. Qin and D. Costinett, "Multi-layer Non-uniform Series Self-resonant Coil for Wireless Power Transfer," *2019 IEEE Energy Conversion Congress and Exposition (ECCE)*, Baltimore, MD, USA, 2019, pp. 3333-3339.

[9] M. Mohammad, E. T. Wodajo, S. Choi and M. E. Elbuluk, "Modeling and Design of Passive Shield to Limit EMF Emission and to Minimize Shield Loss in Unipolar Wireless Charging System for EV," in *IEEE Transactions on Power Electronics*, vol. 34, no. 12, pp. 12235-12245, Dec. 2019.

[10] H. Zhao et al., "Shielding Optimization of IPT System Based on Genetic Algorithm for Efficiency Promotion in EV Wireless Charging Applications," in *IEEE Transactions on Industry Applications*, vol. 58, no. 1, pp. 1190-1200, Jan.-Feb. 2022

[11] B. Zhang, R. B. Carlson, V. P. Galigekere, O. C. Onar and J. L. Pries, "Electromagnetic Shielding Design for 200 kW Stationary Wireless Charging of Light-Duty EV," 2020 IEEE Energy Conversion Congress and Exposition (ECCE), 2020, pp. 5185-5192.

[12] S. Kim, H. -H. Park, J. Kim, J. Kim and S. Ahn, "Design and Analysis of a Resonant Reactive Shield for a Wireless Power Electric Vehicle," in *IEEE Transactions on Microwave Theory and Techniques*, vol. 62, no. 4, pp. 1057-1066, April 2014.

[13] S. Y. Choi, B. W. Gu, S. W. Lee, W. Y. Lee, J. Huh and C. T. Rim, "Generalized Active EMF Cancel Methods for Wireless Electric Vehicles," in IEEE Transactions on Power Electronics, vol. 29, no. 11, pp. 5770-5783, Nov. 2014.

[14] M. Lu and K. D. T. Ngo, "Attenuation of Stray Magnetic Field in Inductive Power Transfer by Controlling Phases of Windings' Currents," in IEEE Transactions on Magnetics, vol. 53, no. 9, pp. 1-8, Sept. 2017.

[15] SAEJ2954. "Wireless Power Transfer for Light-Duty Plug-in/Electric Vehicles and Alignment Methodology." [online] available: https://www.sae.org/standards/content/j2954_202010.

[16] L. Gu, G. Zulauf, A. Stein, P. A. Kyaw, T. Chen and J. M. R. Davila, "6.78-MHz Wireless Power Transfer With Self-Resonant Coils at 95% DC–DC Efficiency," in *IEEE Transactions on Power Electronics*, vol. 36, no. 3, pp. 2456-2460, March 2021.

[17] R. Qin, J. Li and D. Costinett, "A High Frequency Wireless Power Transfer System for Electric Vehicle Charging Using Multi-layer Nonuniform Self-resonant Coil at MHz," *2020 IEEE Energy Conversion*

Congress and Exposition (ECCE), Detroit, MI, USA, 2020, pp. 5487-5494.

[18] R. Qin, J. Li and D. Costinett, "A 6.6-kW High-Frequency Wireless Power Transfer System for Electric Vehicle Charging Using Multilayer Nonuniform Self-Resonant Coil at MHz," in *IEEE Transactions on Power Electronics*, vol. 37, no. 4, pp. 4842-4856, April 2022.

[19] J. Sun, R. Qin, J. Li, D. J. Costinett and L. M. Tolbert, "Design of a Resonant Reactive Shielding Coil for Wireless Power Transfer System," 2021 IEEE Applied Power Electronics Conference and Exposition (APEC), 2021, pp. 1565-1572.

[20] D. C. Meeker, Finite Element Method Magnetics, Version 4.2 (28Feb2018 Build), http://www.femm.info.

[21] DMEGC, "New Soft Magnetic Material Introduction," [Online]. Available:https://www.dmegc.de/file_folder/2019_DMEGC_Soft_Magnetic_material_introduction_English.pdf

[22] García-Moreno, S. and M. Bandala-Sánchez, “Fringing capacitance in sections of circular parallel plates with variable overlapping area,” *Electronics Letters* 49(11): 712-714, 2013

[23] A. Nabih, R. Gadelrab, Q. Li and F. C. Lee, "Dimensional Effects of Core Loss and Design Considerations for High Frequency Magnetics," *2021 IEEE Energy Conversion Congress and Exposition (ECCE)*, 2021, pp. 5488-5495.